March 1986 LIDS-P-1548

MULTIVARIABLE CONTROL OF A SUBMERSIBLE USING THE LQG/LTR DESIGN METHODOLOGY[1]

by

Richard J. Martin[2]
Lena Valavani[3]
Michael Athans[4]

---

1. Research was conducted at the MIT Laboratory for Information and Decision Systems, with support from the Office of Naval Research under contract ONR/N00014-82-K-0582 (NR 606-003).

2. Now at Naval Sea Systems Command, Code 55W31, Washington DC 20362 -5101.

3. Assistant Prefessor, Department of Aeronautics and Astronautics, MIT, Cambridge, Mass. 02139.

4. Professor, Department of Electrical Engineering and Computer Science, MIT, Cambridge, MA 02139.

Reprinted from Proceedings American Control Conference, Seattle, WA, June 1986.

This paper has also been submitted for publication to the IEEE Transactions on Automatic Control.

MULTIVARIABLE CONTROL OF A SUBMERSIBLE USING THE LQG/LTR DESIGN METHODOLOGY[1]

Richard James Martin[2]
Lena Valavani[3]
Michael Athans[4]

ABSTRACT

A multivariable feedback control system is designed for a submersible. The control variables are the bow, rudder, and differential stern control surfaces; these are dynamically coordinated so as to cause the vehicle to follow independent and simultaneous commanded changes in yaw rate, depth rate, pitch attitude, and roll angle. Two designs were evaluated using a nonlinear submersible simulation. One used all four control variables so that active roll control was possible. The other used only three control variables, and active roll control was not employed. Both feedback systems were designed using the Linear Quadratic Gaussian (LQG) with Loop Transfer Recovery (LTR) design methodology so as to meet similar design specifications in the frequency domain. Both the linearized models, and the non-linear simulation have shown that active roll control yields a very significant improvement in submersible performance. Active roll control minimized unwanted depth changes in difficult commanded trajectory scenarios.

INTRODUCTION

This paper summarizes the results of a feasibility study, (1), related to the design of multivariable feedback control systems for deeply submerged submersibles. Present submersibles have minimal automatic control capabilities. Research and development efforts are underway to examine the benefits of closed loop control for maneuvering submersibles. A key issue that has received little attention is: what are the benefits of providing for independent active roll control of a submersible by modification of the stern control surfaces? The objective of our feasibility study was to examine this important issue.

The model of the submersible used in this study uses a rudder and stern plane configuration of the so-called cruciform type. Submersibles use a cruciform stern with mechanically slaved upper and lower rudders, and mechanically slaved port and starboard stern planes. The advantage of this cruciform stern plane configuration is that it allows for intuitive actions on the part of a human operator for desired ship motion. For example, if it is desired to rise or dive, all the human operator has to do is command rise or dive on the stern planes. A similar situation occurs if the operator desires to turn.

A major drawback to this stern configuration is that there is no opportunity to actively control the submersible roll angle. A submersible has a natural tendency to roll by a significant amount during a turn. The so-called "snap roll" of a turning submarine is a nonlinear function of the speed and the rudder displacement angle, and is induced by complex hydrodynamic forces and moments. The detrimental effects of non-zero roll angles are due to the fact that they result in undesirable depth changes, and it becomes even more difficult to turn while, at the same time, maintaining a desired pitch and/or depth rate command. Hence, if methods are utilized to reduce the snap roll, the ability to maintain ordered depth during a maneuver is greatly enhanced. It is important to keep in mind that the large length of a submersible (over three hundred feet) translates to a very limited tolerance for depth errors that compromise the safety of the submersible and/or its missions.

By unslaving the port and starboard planes, and by commanding their deflections independently, it is possible to actively control the submersible roll angle while maintaining pitch control. Also, the deflections of the bow (fairwater) plane can be coordinated with those of the stern planes to provide additional control in the longitudinal axis. It is obviously hard for a human operator to command coordinated changes in four control surfaces simultaneously. This provides the motivation for studying the automatic multivariable feedback control problem for maneuvering.

The majority of previous controller designs for submersibles used classical single-input single-output (SISO) techniques, decoupling the longitudinal and lateral axes, and using only stern and rudder control. There have been a limited number of multi-input multi-output (MIMO) designs for full scale submersibles that can be found in the open

1. Research conducted at the MIT Laboratory for Information and Decision Systems, with support provided by the Office of Naval Research under Contract ONR/N00014-82-K-0582(NR606-003).

2. Naval Sea Systems Command, Code 55W31, Washington, D. C. 20362.

3. Department of Aeronautics and Astronautics, MIT, Cambridge, MA 02139.

4. Department of Electrical Engineering and Computer Science, MIT, Cambridge, MA 02139.

literature, (4)-(8). In these studies active control of the roll angle, using differential stern plane deflections, was not considered.

In this paper we use the MIMO LQG/LTR design methodology, (2), (3), to design two multivariable feedback control systems. One design utilizes independent control of the port and starboard stern planes to achieve active roll control, while the other design does not. The two feedback systems are supposed to cause the submersible to follow demanding maneuvering trajectories in response to simultaneous commands in desired pitch, depth rate, and yaw rate. The desired roll angle is zero. Similar command-following specifications were posed for both designs in the frequency domain. The bandwidth was selected so that excessive saturation of the control surfaces was avoided. In both cases the design model for the submersible was obtained by linearizing the nonlinear differential equations of motion at high speed. The resulting LQG/LTR designs were evaluated using a full-scale nonlinear simulation of the submersible dynamics at the Charles Stark Draper Laboratory.

The simulation results demonstrate that the use of active roll control can have a very significant impact on the performance of the submersible, even in difficult turning maneuvers for a human operator. Active roll control can reduce, by a least a factor of two, undesirable depth excursions when compared to the design that does not actively control the snap roll. Also we have found that the LQG/LTR compensator is quite robust to the changes in the submersible dynamics during a maneuver, where actual speeds can drop by as much as 35 percent. Thus we conjecture that a full-envelope design can be confidently carried out by simply gain-scheduling the parameters of the LQG/LTR compensator as a function of measured submersible forward speed, along the lines suggested by Lively, (4).

The remainder of this paper is organized as follows. Section 2 overviews the modeling issues and the definition of the linearized dynamics used to design the feedback controller. In Section 3 we present the step-by-step procedure that we have used to derive the multivariable LQG/LTR compensators; we augment the natural submersible dynamics with integrators so as to enforce zero steady-state errors to constant commands and/or disturbances. The quality of the linearized designs is judged by the shapes of the singular values of the loop and closed-loop transfer function matrices in the frequency domain. We show how to select the weighting matrices associated with the LQG/LTR design so that the desired target designs, defined by the singular values of the Kalman Filter loop, have identical behavior at both low and high frequencies. Section 4 presents and interprets the results of the nonlinear simulations and contains a discussion of the quantitative benefits of using active roll control.

In closing, we stress that the results presented in this paper represent only a limited feasibility study on the potential benefits of using multivariable control in general, and of active roll control in particular, for full scale submersibles. The resultant LQG/LTR designs must be further refined and analyzed before they are implemented in an actual submersible control system.

MODELING

The controller design procedure begins with the expression of the equations of motion in linear time invariant state space form. The nonlinear, multivariable system that represents the submersible is described by:

$$\frac{d}{dt}\underline{x}(t) = \underline{f}(\underline{x}(t),\underline{u}(t)) \qquad (1)$$

$$\underline{y}(t) = g(\underline{x}(t))$$

where:

$\underline{x}(t)$ is the state vector
$\underline{u}(t)$ is the control vector
$\underline{y}(t)$ is the output vector

The state vector for the submersible must include the six degrees of freedom from the vehicle coordinate system, the desired position variables to locate the submersible with respect to a fixed coordinate system, and the three Euler angles which describe the relationship of the motion of the submersible with respect to the two coordinate systems. Figure 1 shows the submersible reference system used. References (9) to (12) provide guidance on the development of the submarine dynamics.

TABLE 1 DEFINITIONS OF SUBMERSIBLE STATES AND CONTROL VARIABLES

Submersible States

$u = x_1(t)$	forward velocity	(ft/sec)
$v = x_2(t)$	lateral velocity	(ft/sec)
$w = x_3(t)$	vertical velocity	(ft/sec)
$p = x_4(t)$	roll rate	(rad/sec)
$q = x_5(t)$	pitch rate	(rad/sec)
$r = x_6(t)$	yaw rate	(rad/sec)
$\phi = x_7(t)$	roll angle	(radians)
$\theta = x_8(t)$	pitch angle	(radians)

Control Variables

δb	bow/fairwater planes	(radians)
δr	rudder deflection (+ left)	(radians)
δs_1	port stern plane defection (+ down)	(radians)
δs_2	starboard stern plane deflection (+ down)	(radians)

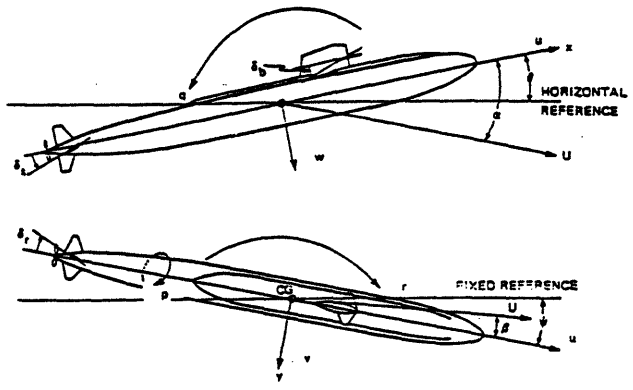

Figure 1 Sketch showing positive directions of axes, angles, velocities, forces, and moments

These nonlinear differential equations can then be linearized through the following fairly straightforward numerical technique. A nominal point is chosen for the design by integrating the nonlinear equations of motion using a specified set of initial conditions. An equilibrium point is found that corresponds to minimum accelerations for all the state variables determined from the integration of the equations of motion. The values of the state variables at the equilibrium point then specify a nominal point, about which higher order terms may be neglected. From these results, a set of linear differential equations may then be produced, the $\underline{A}$ and $\underline{B}$ matrices calculated, and a state space description of the submersible model produced.

The nominal point chosen for this research corresponds to a level submersible trajectory at high speed. The rudder deflection, δr, can be set at arbitrary angles to cause the submersible to turn at different rates, and to roll at different angles. This attempts to determine the open loop sensitivity of the submersible to roll, which has a significant effect on the depth of a submersible in a turning maneuver.

For each nominal point determined, the resulting linear model was validated by perturbing the nominal point of the linear and nonlinear models, and comparing the time histories of the state parameters. Provided the perturbations are not excessive, the nonlinear model will return to the equilibrium point. The linear model, however, will not return to its equilibrium point resulting from the non-zero forces imposed by the control forces, and the absence of nonlinear hydrodynamic effects.

The comparisons of selected nonlinear and linear models and state variables showed excellent correlation, thus validating the linearized models. For further details, refer to reference (1).

Since it is desired to control the submersible during maneuvering situations, a rate controller will be investigated. The four output variables selected are depth rate $\dot{z}$, yaw rate $\dot{\psi}$ roll angle ϕ, and pitch angle θ.

With the output variables determined, and the $\underline{A}$ and $\underline{B}$ matrices calculated from the linearization, the state space description of the model is now complete and takes the form

$$\begin{aligned} \dot{\underline{x}}(t) &= \underline{A}\,\underline{x}(t) + \underline{B}\,\underline{u}(t) \\ \underline{y}(t) &= \underline{C}\,\underline{x}(t), \end{aligned} \tag{2}$$

where the output vector $\underline{y}(t)$ is given by

$$\underline{y}(t) = \left[\phi(t) \quad \theta(t) \quad \dot{\psi}(t) \quad \dot{z}(t)\right]^T . \tag{3}$$

As mentioned previously, there are four possible control variables. These are δs_1, δs_2, δr, and δb. Figure 2 illustrates the control surface configurations used in this research.

The use of modal analysis allowed the formulation of the prerequisites necessary to pursue the LQG/LTR design methodology. These prerequisites are that the open loop linear model be detectable and stabilizable, and that the location of nonminimum phase zeros be known. For a detailed description of the analysis of the linear model, refer to reference (1). The numerical values for the $\underline{A}$ and $\underline{B}$ matrices are included in Appendix A. The open-loop model of the linearized submersible dynamics is stable and minimum-phase.

The final issue associated with the linear model is that of scaling. It is now widely appreciated that in multivariable designs the control and output variables must be scaled so that controls and tracking errors, expressed in different physical units, can be compared fairly.

The scaled control variables were established as follows. We used physical saturation limits on the control surfaces: 20 degrees for the bow planes, 30 degrees for the rudder, and 25 degrees for the stern planes. After transforming from radians to degrees, the scaled controls were set as follows:

one unit of bow = 0.667 units of rudder
= 0.8 units of stern.

The scaled outputs were first derived by changing radians to degrees. Then, in terms of the performance of the control system, it was judged that a 1 deg/sec error in either yaw rate or depth rate was 10 times more serious than a 1 degree error in roll or pitch angle. Thus the scaled outputs were set as follows:

one unit of pitch = one unit of roll
= 0.1 unit of yaw rate
= 0.1 unit of depth rate.

The resultant scaled model was used in the designs that will be described in the sequel.

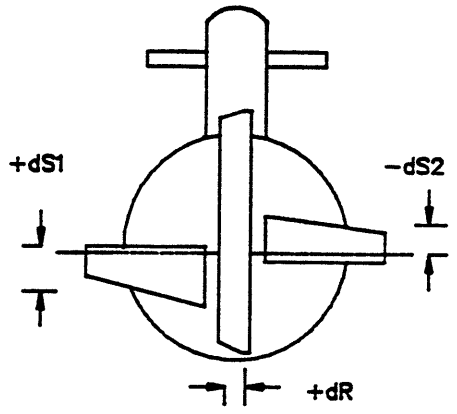

Figure 2 View from Stern Showing Rudder and Differential Sternplanes

MULTIVARIABLE CONTROL SYSTEM DESIGN

Introduction

As stated earlier, a controller is designed using the LQG/LTR design methodology. The singular value loop shaping approach is used to obtain desirable singular values of the system transfer function matrix to meet the specifications of performance and robustness to plant uncertainties and modeling errors.

Controller Specifications

Performance specifications outlined in this research are not all encompassing and reflect a simplified submersible control system. The performance requirements are driven by the intuitive engineering approach to obtain good command following, good system response, robustness, and disturbance rejection. These performance requirements are met through loop shaping techniques.

Two performance requirements are imposed on the controller design. First, the steady state error to step commands and step disturbances is to be zero. Second, the maximum crossover frequency is limited by the ability of the submersible to respond and by the rate at which the compensator deflects the control surfaces.

The zero steady state requirement is met by placing integrators in each of the control channels. This is necessitated because we plan to use the version of the LQG/LTR design methodology which breaks the loop at the plant output, or equivalently, at the error channel. In this manner, the integrators will then become part of the compensator which precedes the plant in the feedback loop. Note that the use of integral control in the input channels does not prevent the specification for maximum crossover frequency from being met.

The maximum crossover frequency of the compensator determines the rapidity of the control surface deflections based on the error signals which are generated by the difference between the reference commands and the measured outputs, and was selected to be in the neighborhood of 0.5 rad/sec. based on desired actuator dynamics and saturation limits (1). Although not explicitly stated as a performance specification, from the performance aspect, it is desirable to have all singular values cross over at about the same frequency. Also, on the high frequency side, the controller must be capable of rejecting noise and be robust to high frequency modeling errors. Noise sources generally originate from the environment, or from the sensor itself. Sensor noise typically occurs at a higher frequency than the system bandwidth and should not affect the dynamics of the submersible since ship eigenvalues will typically lie in the lower frequency band.

The LQG/LTR Design Methodology

The multivariable LQG/LTR design methodology consists of four major steps (2), (3).

The first step is the development of a low frequency model of the nominal plant and determination of modeling uncertainties.

The modeling uncertainty in the nominal model due to sensor noise, unmodeled submersible dynamics, and actuator dynamics, is assumed to be concentrated at high frequencies (in this study, higher than 10 rad/sec). Fixing the crossover frequency of the singular values of the loop transfer function matrix will determine the significance of the unmodeled dynamics, and the ability of the plant to meet command following specifications.

The second step of the design process establishes the low frequency performance requirements. The state space block diagram of the compensated plant is shown in Figure 3.

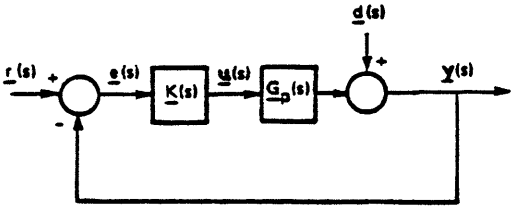

Figure 3 Block Diagram of a MIMO Compensated Plant

where:

$\underline{r}(s)$ = reference signal or command input vector
$\underline{e}(s)$ = error signal vector
$\underline{u}(s)$ = control vector to the plant
$\underline{y}(s)$ = output vector of the plant
$\underline{d}(s)$ = disturbance vector at the plant output
$\underline{K}(s)$ = compensator transfer function matrix
$\underline{G}(s)$ = augmented plant transfer matrix

The transfer matrix $\underline{G}(s)$ contains the nominal low frequency model $\underline{G}_p(s)$ and any augmenting

dynamics $\underline{G}_a(s)$, and is defined the nominal design model. Thus

$$\underline{G}(s) = \underline{G}_p(s)\ \underline{G}_a(s) \qquad (4)$$

Augmenting the dynamics of the submersible control system normally serves a dual purpose. One is to partially model the actuator dynamics to make the model as accurate as possible and to achieve desirable rolloff beyond crossover for stability-robustness. The other is to include integrators to cause the compensator to permit the submersible to achieve zero steady state error to step inputs and disturbances (i.e., perfect command following at DC). The actuator dynamics are above the maximum expected crossover frequency, and thus are neglected. This is perfectly valid as long as the rolloff above crossover is fast enough and satisfies the robustness criteria.

A block diagram of the augmented model appears in Figure 4. It is seen that the integrators are placed in the control channels. The mathematics of the augmented states are manipulated in such a way as to provide a means to achieve the desired Kalman Filter open loop shapes $\underline{G}_{FOL}(s)$.

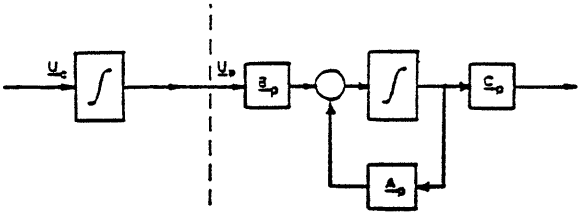

Figure 4 Integrators Placed in the Control Channel of Plant

We define the augmentation dynamics by $\underline{G}_a(s)$, whose state space description is

$$\dot{\underline{u}}_p(s) = \underline{u}_c(s)\ ;\ \underline{G}_a(s) = \underline{I}/s$$

where each matrix is $[4 \times 4]$. The augmenting integrator dynamics are added to the 8^{th} order system producing a 12^{th} order system. Note that the physical input to the plant is labelled $\underline{u}_p(s)$ to distinguish it from the output of the compensator $\underline{u}_c(s)$. Although the augmentation dynamics $\underline{G}_a(s)$ will eventually be lumped with the compensator, they are kept separate until the LQG/LTR procedure is complete.

To determine the requirements of $\underline{K}(s)$, the overall loop transfer function of the closed loop system is analyzed, where

$$\underline{y}(s)=[\underline{I}+\underline{G}(s)\underline{K}(s)]^{-1}\underline{d}(s)+[\underline{I}+\underline{G}(s)\underline{K}(s)]^{-1}\underline{G}(s)\underline{K}(s)\underline{r}(s). \qquad (5)$$

For good command following, $\underline{y}(s) \approx \underline{r}(s)$, and for disturbance rejection, the effect of $\underline{d}(s)$ must be kept small. If the minimum singular value of $\underline{G}(s)\underline{K}(s)$ is large with respect to unity at frequencies below crossover, both of these requirements can be met. Likewise, for frequencies above crossover, the response of the outputs with respect to sensor noise can be minimized and stability-robustness enhanced if the maximum singular value of $\underline{G}(s)\underline{K}(s)$ is small with respect to unity.

Combining the above conditions, we essentially impose high and low frequency barriers on the singular value plots of the loop transfer function matrix $\underline{G}(s)\underline{K}(s)$, as shown in Figure 5.

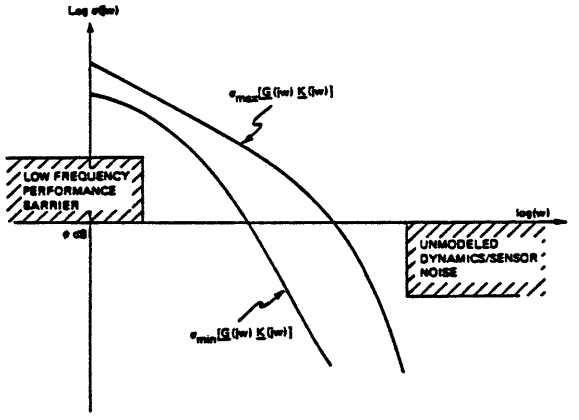

Figure 5 Plot of Desired Singular Value Shapes

The high frequency barrier imposes a robustness constraint on the compensator and the low frequency barrier imposes the command following and disturbance rejection requirements.

The third step of the design process is determining the compensator transfer function matrix, $\underline{K}(s)$, that will provide the desired singular values of $\underline{G}(s)\underline{K}(s)$. This step of the process is appropriately termed "loop shaping".

The Kalman Filter (KF) methodology is first applied to the nominal design model. This produces a transfer matrix $\underline{G}_{KF}(s)$ that has the desired singular value loop shapes; thus is called the "target design". A distinction is noted in this procedure, however, because the KF theory is applied in a specific manner which is not to be confused with optimal state estimation.

$$\begin{aligned} \dot{\underline{x}}(t) &= \underline{A}\ \underline{x}(t) + \underline{B}\ \underline{u}(t) \\ \underline{y}(t) &= \underline{C}\ \underline{x}(t)\ . \end{aligned} \qquad (6)$$

This description is modified to reflect the (fictitious) process and measurement noises

$$\begin{aligned} \dot{\underline{x}}(t) &= \underline{A}\ \underline{x}(t) + \underline{L}\ \underline{\xi}(t) \\ \underline{y}(t) &= \underline{C}\ \underline{x}(t) + \underline{\theta}(t), \end{aligned} \qquad (7)$$

where:

$\underline{\xi}(t)$ = process white noise with $\underline{I}$ intensity matrix

$\underline{\theta}(t)$ = measurement white noise with $\mu\underline{I}$ intensity matrix.

The design parameters μ and $\underline{L}$ are used to produce the desired loop shapes of the transfer matrix $\underline{G}_{KF}(s)$ where

$$\underline{G}_{KF}(s) = \underline{C}[s\underline{I} - \underline{A}]^{-1}\underline{H} \qquad (9)$$

$$H = (1/\sqrt{\mu})\underline{\Sigma}\underline{C}' , \qquad (10)$$

and $\underline{\Sigma}$ is the solution to the Filter Algebraic Riccatti Equation (FARE)

$$0 = \underline{A\Sigma} + \underline{\Sigma A}' + \underline{LL}' - (1/\sqrt{\mu})\underline{\Sigma C}'\underline{C\Sigma} . \qquad (11)$$

For a specific value of μ, the transfer matrix $\underline{G}_{KF}(s)$ can be approximated quite readily. Since at high and low frequencies $s = j\omega$, we have the approximation (2), (3)

$$\underline{G}_{KF}(s) \approx (1/\sqrt{\mu})\underline{G}_{FOL}(s), \text{ for}$$

$$\underline{G}_{FOL}(s) = \underline{C}[s\underline{I} - \underline{A}]^{-1}\underline{L}, \text{ then} \qquad (12)$$

$$\sigma_i[\underline{G}_{KF}s)] \approx (1/\sqrt{\mu})\sigma_i[\underline{G}_{FOL}(s)] ,$$

then the $\underline{L}$ matrix (design parameter) can be chosen in a way to produce the desired loop shapes and μ can then be used to adjust the singular values up or down to meet the required crossover frequency specifications.

As long as $[\underline{A},\underline{L}]$ is stabilizable and $[\underline{A},\underline{C}]$ is detectable, then any choice of μ and $\underline{L}$ will provide the following guaranteed properties for the "target design" $\underline{G}_{KF}(s)$:

1. closed loop stable
2. robustness and performance guarantees:

   $\sigma_{min}[\underline{I} + \underline{G}_{KF}(s)] > 1$

   $\sigma_{min}[\underline{I} + \underline{G}_{KF}^{-1}(s)] > 1/2$
3. infinite upward gain margin
4. 6 dB downward gain margin
5. ±60° phase margins

In our design, we decided to select $\underline{L}$ so that all singular values of the target design $\underline{G}_{KF}(j\omega)$ are identical at low and high frequencies, thus hoping that all singular values will cross at about the same frequency. To find the numerical value of $\underline{L}$ that will accomplish this we proceed as follows.

Recall that $\underline{G}(s) = \underline{G}_p(s)\underline{G}_a(s)$, and define $\underline{G}(s) = \underline{C}[s\underline{I} - A]^{-1}\underline{B}$, where

$$\underline{A} = \begin{bmatrix} \underline{0} & \underline{0} \\ \underline{B}_p & \underline{A}_p \end{bmatrix} \qquad \underline{C} = [\underline{0} \;\; \underline{C}_p],$$

$$s\underline{I}-\underline{A} = \begin{bmatrix} s\underline{I} & \underline{0} \\ -\underline{B}_p & s\underline{I}-\underline{A}_p \end{bmatrix} , \text{ and}$$

$$[s\underline{I}-\underline{A}]^{-1} = \begin{bmatrix} \underline{I}/s & \underline{0} \\ [s\underline{I}-\underline{A}_p]^{-1}\underline{B}_p/s & [s\underline{I}-\underline{A}_p]^{-1} \end{bmatrix} .$$

At low frequencies, $s\underline{I}-\underline{A}_p \approx -\underline{A}_p$ and $[s\underline{I}-\underline{A}_p]^{-1} \approx -\underline{A}_p{}^{-1}$. Since $\underline{A}_p$ has distinct and non-zero eigenvalues, $\underline{A}_p{}^{-1}$ exists. We now partition the $\underline{L}$ matrix into $\underline{L}_1$ and $\underline{L}_2$, where $\underline{L}_1$ will be selected for matching the singular values at low frequency and $\underline{L}_2$ will be selected for matching the singular values at high frequency.

Forming $\underline{G}_{FOL}(s)$ for low frequencies,

$$\underline{G}_{FOL}(s) = \underline{C}[s\underline{I}-\underline{A}]^{-1}\underline{L}$$

$$\underline{G}_{FOL}(s) \approx [\underline{0} \;\; \underline{C}_p]\begin{bmatrix} \underline{I}/s & \underline{0} \\ -\underline{A}_p{}^{-1}\underline{B}_p/s & -\underline{A}_p{}^{-1} \end{bmatrix}\begin{bmatrix} \underline{L}_1 \\ \underline{L}_2 \end{bmatrix}$$

$$\approx -\underline{C}_p\underline{A}_p{}^{-1}\underline{B}_p\underline{L}_1/s - \underline{C}_p\underline{A}_p{}^{-1}\underline{L}_2 . \qquad (13)$$

It is now seen that the singular values can be matched at low frequencies if we select the matrix $\underline{L}_1$ as follows:

$$\underline{L}_1 = -[\underline{C}_p\underline{A}_p{}^{-1}\underline{B}_p]^{-1} . \qquad (14)$$

At high frequencies, $s\underline{I}-\underline{A}_p \approx s\underline{I}$, and $[s\underline{I}-\underline{A}_p]^{-1} \approx \underline{I}/s$. Forming $\underline{G}_{FOL}(s)$ for high frequencies,

$$\underline{G}_{FOL}(s) = [\underline{0} \;\; \underline{C}_p]\begin{bmatrix} \underline{I}/s & \underline{0} \\ \underline{B}_p/s^2 & \underline{I}/s \end{bmatrix}\begin{bmatrix} \underline{L}_1 \\ \underline{L}_2 \end{bmatrix}$$

$$\approx \underline{C}_p\underline{B}_p\underline{L}_1/s^2 + \underline{C}_p\underline{L}_2/s .$$

The singular values can now be matched at high frequencies if we select $\underline{L}_2$ as follows:

$$\underline{L}_2 = \underline{C}_p'(\underline{C}_p\underline{C}_p')^{-1}, \qquad (15)$$

since as $s \to \infty$, $1/s > 1/s^2$, and the second term dominates the maximum singular values.

The above method for constructing the $\underline{L}$ matrix provides the designer with a guarantee of identical behavior of the Kalman Filter loop singular values at both high and low frequencies. However, this method does not provide an opportunity to directly control the shape of the singular values at crossover.

Once the $\underline{L}$ matrix is determined, the design parameter μ is used to move the singular value plots up or down to obtain the desired crossover

frequency. Then we can solve the FARE and calculate $\underline{G}_{KF}(s)$. The final value of μ that we used for the model during the Kalman Filter design process was $\mu = 4$.

The fourth and final step of the LQG/LTR design process involves the "recovery" of the target design $\underline{G}_{KF}(s)$ by the compensated plant transfer matrix $\underline{G}(s)\underline{K}(s)$. This is done by solving the Control Algebraic Riccatti Equation (CARE)

$$0 = -\underline{K}\underline{A} - \underline{A}'\underline{K} - q\underline{C}'\underline{C} + \underline{K}\underline{B}\underline{B}'\underline{K}, \text{ for } q > 0. \quad (16)$$

Using the design parameter q, we solve for the $\underline{K}$ matrix, and determine the control gain matrix

$$\underline{G} = \underline{B}'\underline{K} . \quad (17)$$

For a valid solution of the CARE, three conditions are necessary:

1. $[\underline{A},\underline{B}]$ must be stabilizable,
2. $[\underline{A},\underline{C}]$ must be detectable, and
3. The nominal design plant must not have non-minimum phase zeros.

Providing the plant is minimum phase (3), the singular values of $\underline{G}(s)\underline{K}(s)$ converge to the singular values of $\underline{G}_{KF}(s)$ as the design parameter $q \to \infty$. Above crossover frequencies, additional rolloff is produced by the recovery phase, which further enhances the high frequency robustness characteristics. As a result, the loop shape of $\underline{G}_{KF}(s)$ is approximately recovered, and the resulting controller will have the desired performance characteristics. A value of q = 1000 was used for our model. The minimum and maximum crossover frequencies turned out to be 0.2 rad/sec and 0.5 rad/sec, respectively.

When calculated using the above procedure, the Filter gain matrix $\underline{H}$ and the Control gain matrix $\underline{G}$ define a special type of compensator known as an LQG/LTR Compensator, designated as $\underline{K}(s)$. This compensator differs from other LQG compensators only in the manner in which $\underline{G}$ and $\underline{H}$ are calculated. The state space description of the LQG/LTR compensator is

$$\dot{\underline{z}}(t) = (\underline{A} - \underline{B}\underline{G} - \underline{H}\underline{C})\,\underline{z}(t) - \underline{H}\,\underline{e}(t) \quad (18)$$

$$\underline{u}(t) = -\underline{G}\,\underline{z}(t) , \quad (19)$$

and is shown pictorially in Figure 6.

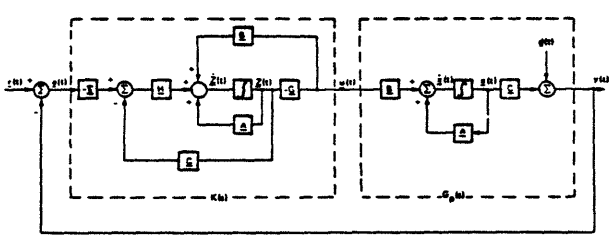

Figure 6 State Space Description of the LQG/LTR Design

Description of the Active Roll Control Design

In the active roll control design we used all four available controls, namely the (scaled) bow, rudder, and differential stern plane deflections. These four independent control variables can be used to command the four (scaled) outputs, i.e., roll angle, pitch angle, yaw rate, and depth rate.

The outcome of the LQG/LTR design for this system is summarized in the singular value plots of Figure 7. Figures 7(c) and 7(d) show how the specific choice of the design matrix $\underline{L}$ impacts the "target design"; notice that at both high and low frequencies all singular values are essentially the same, and that the crossover frequencies are in the same ballpark, as desired. Comparison of Figures 7(d) and 7(e) illustrates how the LTR works. The singular values of the LQG/LTR loop transfer function matrix are very near those of the Kalman filter loop until about 1 rad/sec. After that frequency the singular values roll-off at -40 dB/dec providing extra robustness to high-frequency model errors and sensor noises.

The excellent command-following properties of this design become apparent from Figure 7(f) which shows the singular values of the closed loop system, from command inputs to outputs. Notice that all sinusoidal command inputs at frequencies below 0.1 rad/sec are followed with minimal tracking error.

Description of the Design Without Active Roll Control

If the stern planes are slaved together, then we only have three independent controls, i.e., bow, rudder, and stern control surface deflections. Thus we can independently control three outputs, i.e., pitch angle, yaw rate, and depth rate. We cannot control directly the roll angle, and we must accept whatever roll angle is generated.

Figure 8 provides a summary of the LQG/LTR design for this 3-input 3-output feedback control system. Comparisons of Figures 7 and 8 shows that the resulting feedback system meets essentially the same specifications in the frequency domain as the 4-input 4-output design, except that we have lost our ability to directly influence the roll angle.

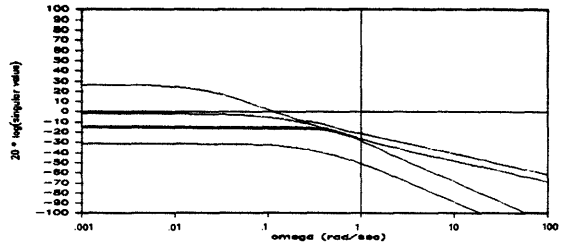

(a) Unaugmented Plant

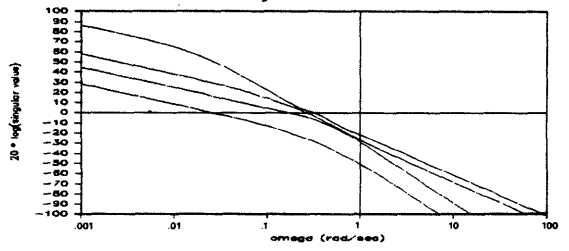

(b) Design Plant augmented with integrators in the control channels

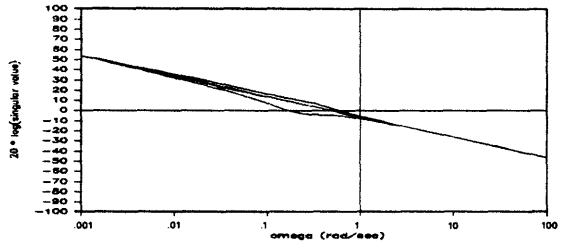

(c) Kalman Filter Open Loop, G_{FOL}

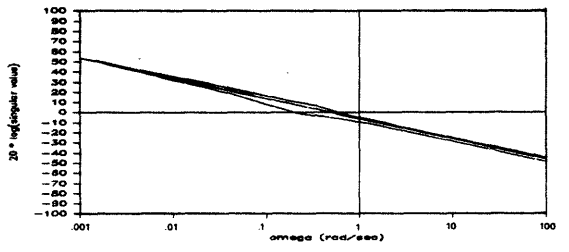

(d) Kalman Filter Loop, G_{KF}; the "target" design

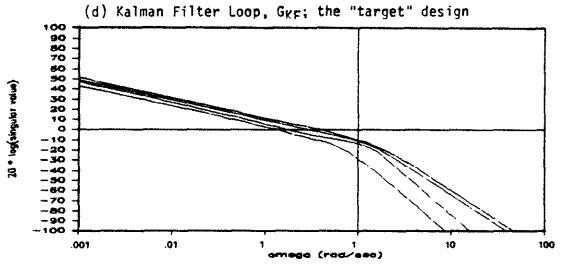

(e) Recovered Loop Transfer Function, G(s)K(s) with q = 1000, using the LQG/LTR Compensator

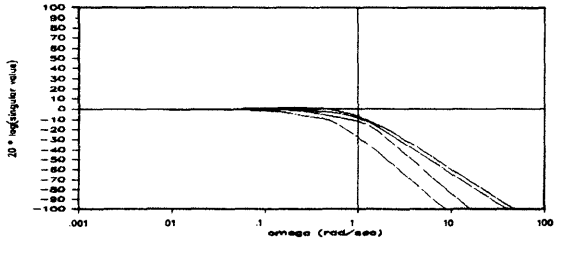

(f) Singular Values of the Closed Loop

Figure 7 Summary of LQG/LTR Design Sequence, Design with Roll Control

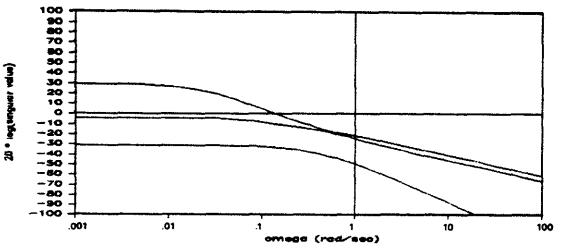

(a) Unaugmented Plant

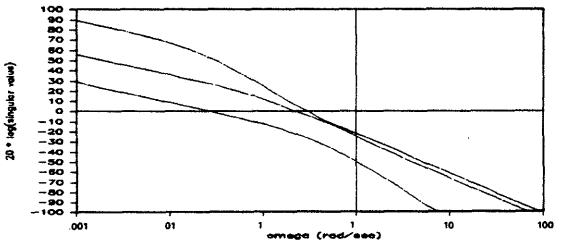

(b) Design Plant augmented with integrators in the control channels

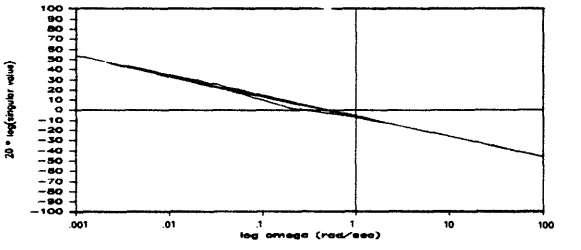

(c) Kalman Filter Open Loop, G_{FOL}

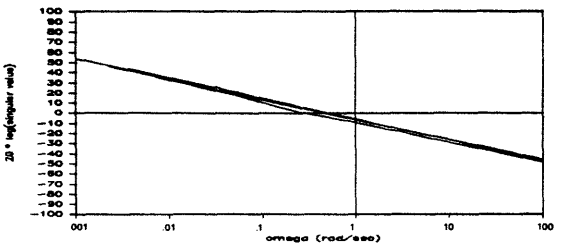

(d) Kalman Filter Loop, G_{KF}; the "target" design

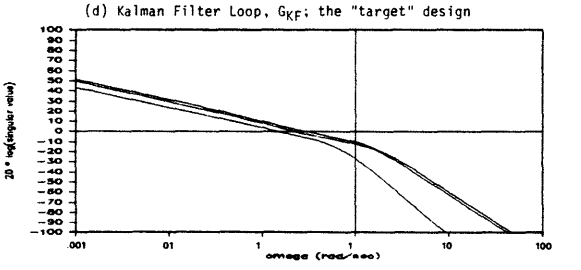

(e) Recovered Loop Transfer Function, G(s)K(s) with q = 1000, using the LQG/LTR Compensator

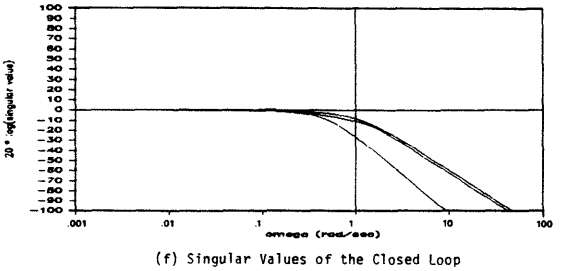

(f) Singular Values of the Closed Loop

Figure 8 Summary of LQG/LTR Design Sequence, Design without Roll Control

NONLINEAR SIMULATIONS

Introduction

The controller designs were tested using both the linear and non-linear submersible simulations to determine how closely the performance specifications are met, and to test for instabilities in the design. In both cases, the compensator designs were shown to be satisfactory.

Active Roll vs Non-roll Control Designs

Having established the validity of the compensator design and the compensator software, it is now necessary to demonstrate the performance characteristics of the active roll control feedback system to the equivalently designed system without roll control capability.

Comparisons are shown for two simulations. The first comparison is for a combined maneuver in which step commands of 1 degree of pitch, 0.5 feet/second of depth rate, and 1 degree/second of yaw rate are provided to the feedback systems. The second simulation is for a commanded yaw rate of 3 degrees/second, and provides additional insight into the differences in the two compensators, and the robustness of the compensator design. The interested reader can find more simulations in (1) and (8).

In both simulations the commands are applied as ramped step inputs at t = 5 seconds.

Combined Maneuver

This maneuver is for step input commands of zero roll angle, -0.5 ft/sec in depth rate, 1 deg/sec in yaw rate, and 1 degree in pitch. Referring to Figure 9, we observe a 6% decrease in the forward velocity.

Looking first at the system with roll control, it is observed that the errors in roll angle and yaw rate are damped by t = 40 seconds. The errors in pitch and depth rate, however, are not damped until t = 140 seconds. By t = 200 seconds, the ship has experienced a depth rise of 80 feet. The stern planes are deflected differentially to counteract the roll moment, with a steady differential deflection of 6°. The bow planes are deflected at -1.5° to maintain the commanded depth rate, and the rudder is deflected at -2° to maintain the commanded yaw rate.

Comparing the design without roll control, it is observed that the ship experiences a snap roll of 10°. This roll angle causes a pitch angle of -2° which results in a large pitch error. In fact, at t = 200 seconds, there is still an error in pitch of 0.5°, or 50% of the commanded pitch angle. This also causes a -0.35 ft/sec depth rate instead of the commanded -.5 ft/sec. The net result of these errors is displayed in the depth of the ship. The depth rise in this design is 25 feet, instead of 80 feet, as in the model with roll control. Note here, that a depth rise of (190 x 0.5 =) 95 ft is commanded.

The steady state stern planes angle is -0.75°, which indicates the stern planes are being used to obtain the ordered pitch angle. Because the depth rate is a result of the combination of pitch angle and ship's speed, we observe the bow planes are essentially being used to attain the ordered depth rate. In the roll control design, the ship obtained the ordered pitch angle rather quickly, thus, the bow planes are deflected in the opposite direction to limit the depth rate to -0.5 ft/sec.

Hard Turning Maneuver

This maneuver is for a commanded yaw rate of 3 deg/sec, and is provided to display the effects of control surface saturation. Referring to Figure 10, we observe a drop in ship's speed of almost 45%. Looking at the design with roll control, it is observed that the ship initially rolls outward approximately 8°, then snaps inward at t = 14 seconds. The maximum downward pitch angle reaches 4° at t = 160 seconds, and starts to reduce by the end of the run. The undesired depth loss in this case is 184 ft. The stern planes again deflect differentially to counteract the roll moment, but now, we observe the port stern planes are deflected at -3.9° at t = 200 seconds whereas the starboard stern planes are deflected at 7.8°. This indicates that the stern planes, although deflecting differentially for roll control, are also being deflected to control the pitch angle. The bow planes are deflected at 6.25° in an attempt to minimize depth rate. To maintain the ordered yaw rate, the rudder is deflected -27° at the end of the run.

Comparing the system without roll control, we observe that the ship snap rolls inboard 19°, and pitch angle approaches -12°. The stern planes deflect to limit depth rate. The bow planes, however, saturate in this run at t = 22 seconds. Up to this point, the ship's depth was maintained fairly well. As soon as the bow planes saturate, the depth rate increases, causing the ship to lose depth. This causes the stern planes to deflect in the opposite direction in an attempt to minimize pitch angle and depth rate. At t = 25 seconds, the pitch angle steadies, and starts to come off. At t = 108 seconds, the depth rate goes negative, and it is observed the bow planes come out of saturation. By t = 200 seconds, we observe that the roll angle has been reduced to 8°, maximum negative pitch angle is 7°, depth rate is significantly reduced, and none of the control surfaces are saturated. Depth at the end of the run is 820 feet, which equates to an undesired depth loss of 320 feet, as compared to the roll control model's depth loss of 184 feet.

The purpose of this run was to demonstrate how different the submersible's trajectory is when the control surfaces saturate, and the stability and robustness of the design. The numerical results demonstrate once more the beneficial consequences of active roll control resulting in significant reduction to undesirable depth changes.

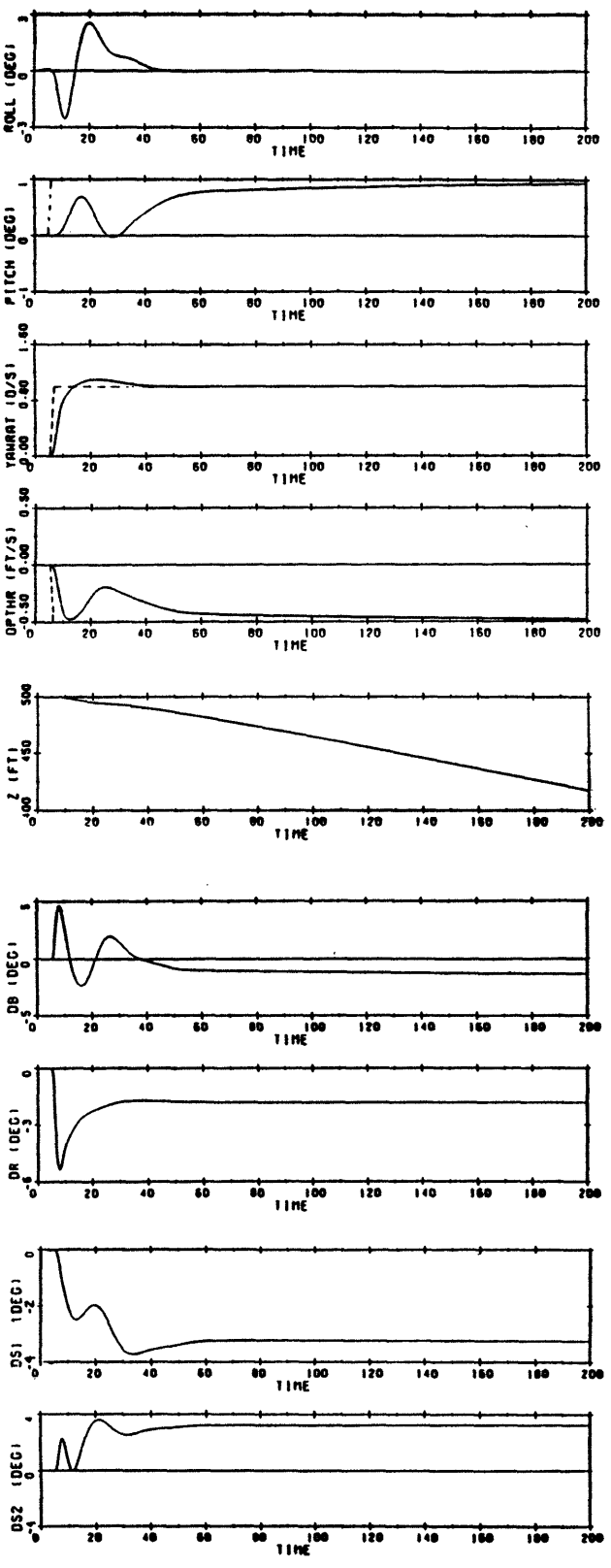

Figure 9(a) Combined Maneuver, Model with Roll Control

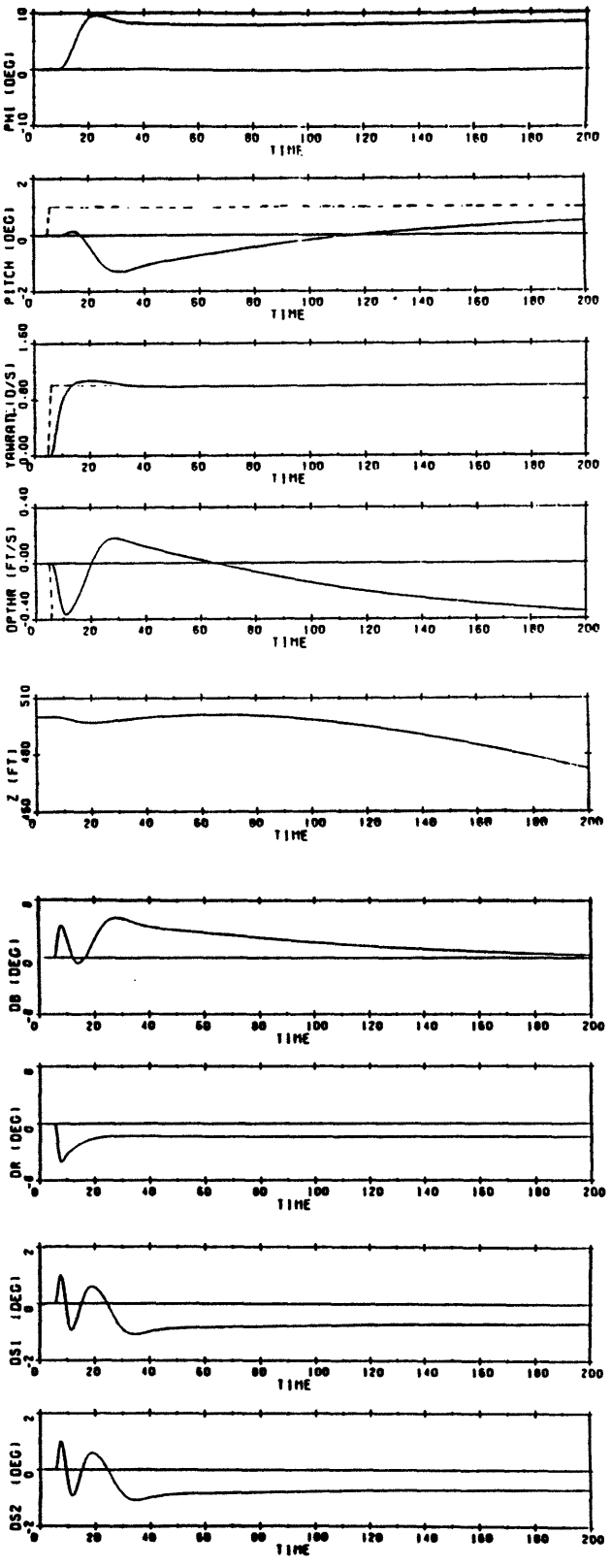

Figure 9(b) Combined Maneuver, Model without Roll Control

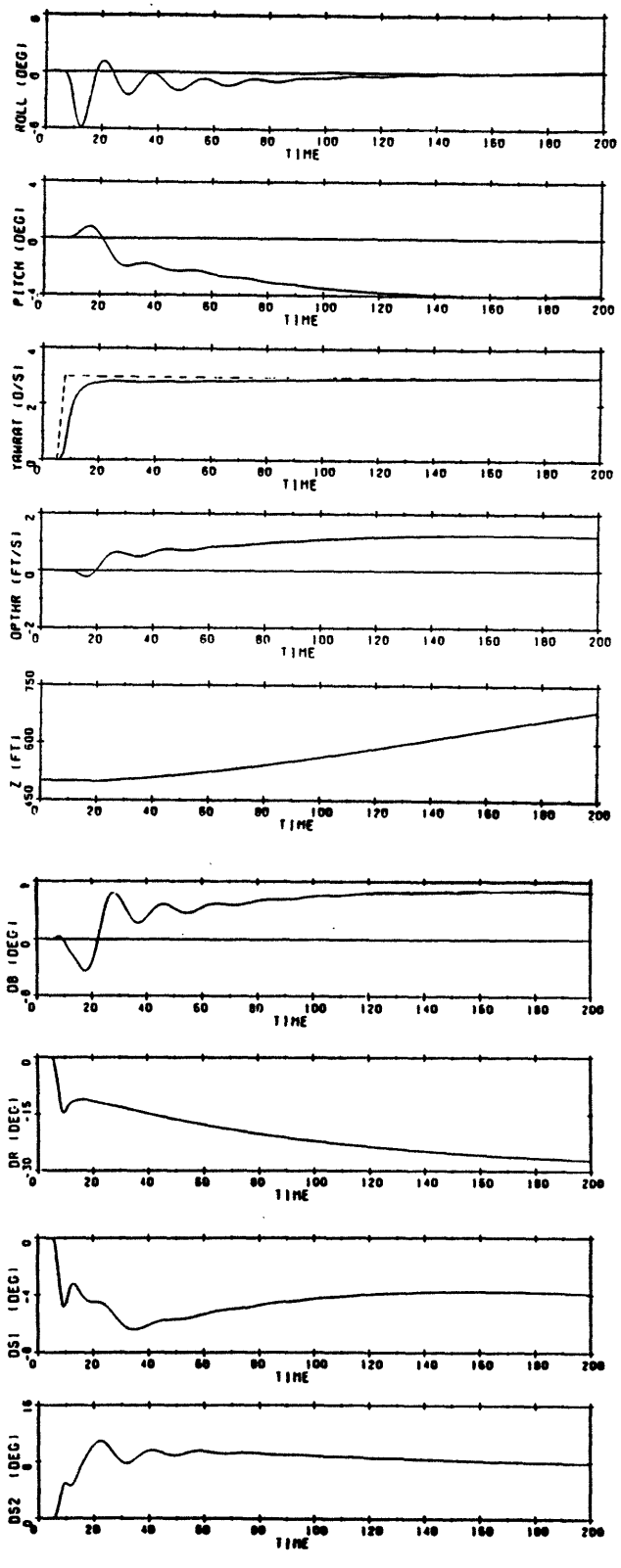

Figure 10(a) Hard Turning Maneuver, Model with Roll Control

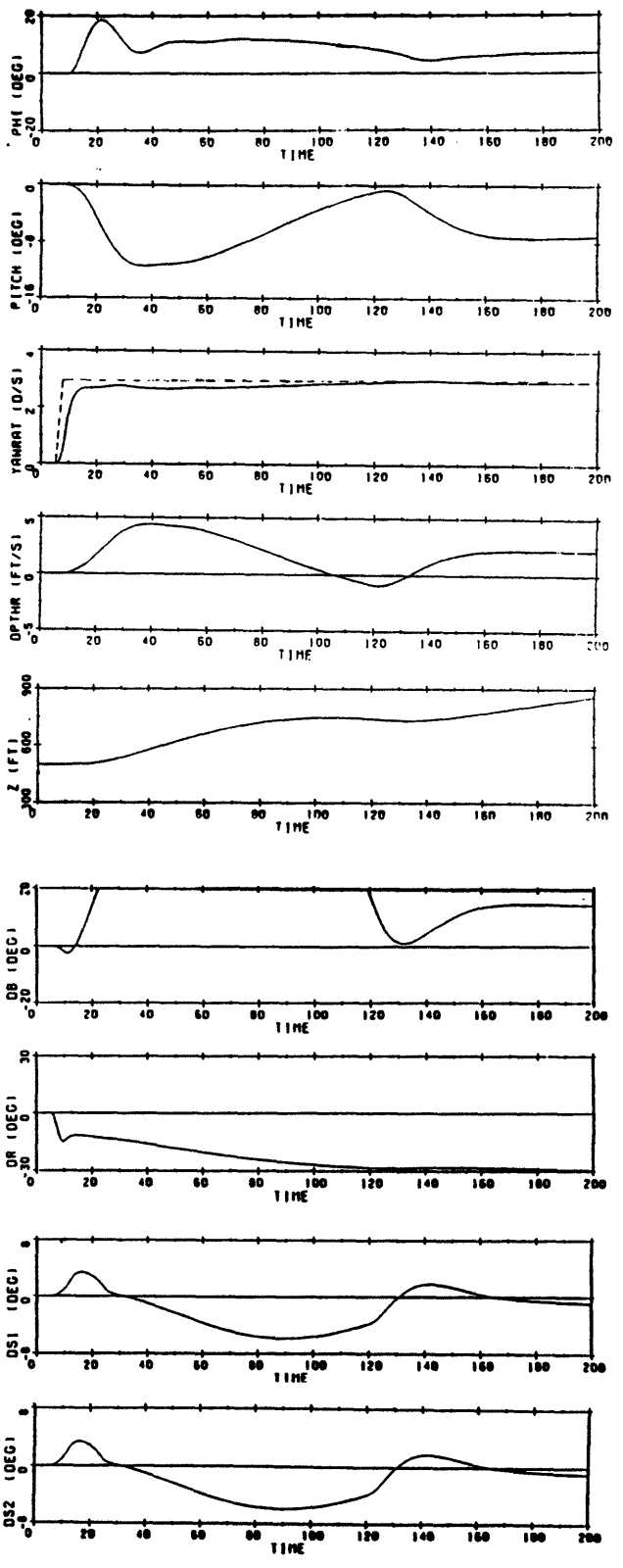

Figure 10(b) Hard Turning Maneuver, Model without Roll Control

CONCLUSIONS

Multivariable control system design using the LQG/LTR methodology has been successfully utilized to design a submersible control system with roll control capability.

The purpose of this paper was to demonstrate the advantages of roll control on a submersible. A limited number of simulations were performed, and the performance of the submersible with roll control is much improved over the design without roll control. The control system was designed for a submersible at high speed, and we observed the control system did fairly well, even for a 45% decrease in forward velocity of the ship. Additionally, the control system was designed using the inertial reference frame rather than the body reference frame of the ship. Use of the fixed inertial coordinate system provided better control of the submersible in maneuvering situations than for previous designs which used the body reference frame.

At this point it is important to stress the following observations:

- The performance characteristics of the submersible with active roll control are enhanced considerably over the design without roll control. The simulations demonstrated considerable depth improvement, and less control surface deflections and saturation in severe maneuvers, as demonstrated in Figure 10.
- This research demonstrates a technique to simulate performance characteristics of "paper" control systems for trade-off studies for specified performance criteria.
- The fact that only small perturbations can be applied in validation of the design is not a limitation of the control design methodology. It is, however, a limitation of the linear model.
- To demonstrate the flexibility a controls engineer has when using multivariable control, the bow/fairwater planes were included in this thesis. Use of the bow/fairwater planes at high speed in current submersibles may not be considered practical due to flow disturbances, and structural limitations.

REFERENCES

1. Martin, R. J. "Multivariable Control System Design For A Submarine Using Active Roll Control", Engineers Thesis, MIT, 1985.
2. Athans, M. Multivariable Control Systems, Course Lecture Notes, MIT, Spring 1984.
3. Doyle, J. C. and Stein, G. "Multivariable Feedback Design: Concepts for a Classical/Modern Synthesis", IEEE Transactions on Automatic Control, Vol. AC-26, No. 1 (February, 1981): pp 4-16.
4. Lively, K. A. "Multivariable Control System Design for a Submarine", Engineers Thesis, MIT, 1984.
5. Dreher, L. J. "Robust Rate Control System Designs for a Submersible", Engineers Thesis, MIT, 1984.
6. Milliken, L. G. "Multivariable Control of an Underwater Vehicle", Engineers Thesis, MIT, 1984.
7. Harris, K. A. "Automatic Control of a Submersible", Masters Thesis, MIT, 1984.
8. Mette, J. A. "Multivariable Control of a Submarine Using the LQG/LTR Method", Engineers Thesis, MIT, 1985.
9. Abkowitz, M. Stability and Motion Control of Ocean Vehicles, MIT Press, Cambridge, MA., 1969.
10. Bonnice, B. and Valavani, L. "Submarine Configuration and Control", CSDL Memo SUB 1-1083, 1983.
11. Gertler, M. and Hagan G. R. "Standard Equations of Motion for Submarine Simulation", Naval Ship Research and Development Report 2510, June 1967.
12. Bonnice, B. CONSTRPS Fortran and Executive Command Computer Programs, CSDL, May 1984.

APPENDIX A

ORIGINAL MATRICES PRIOR TO SCALING

$$\underline{x}^T = [u\ v\ w\ p\ q\ r\ \phi\ \theta]$$

A MATRIX

-3.8245E-02	-2.1911E-02	-2.7720E-03	-1.8964E-02
-2.9363E-01	3.1674E+00	0.0000E+00	2.9326E-04
1.1461E-03	-1.5919E-01	-1.9338E-03	-1.1464E+00
1.1276E-01	-1.5397E+01	1.3004E-01	-1.7564E-03
2.4225E-05	4.6499E-04	-1.0631E-01	-1.5984E+00
1.2070E+01	8.0194E-02	0.0000E+00	7.5597E-03
2.4614E-04	-1.1680E-02	-1.3226E-03	-4.3445E-01
-2.3879E-01	-7.1773E-03	-1.5995E-01	2.1603E-03
-5.3732E-06	-1.8585E-05	1.3207E-03	-1.1380E-02
-4.0755E-01	1.0074E-04	0.0000E+00	-2.4934E-03
-2.7564E-05	-2.0277E-03	2.4063E-05	-8.1034E-03
3.6042E-03	-3.8180E-01	2.5836E-04	-3.4895E-06
0.0000E+00	0.0000E+00	0.0000E+00	1.0000E+00
1.3427E-02	-1.2348E-01	-2.0244E-10	-1.2660E-02
0.0000E+00	0.0000E+00	0.0000E+00	0.0000E+00
9.9414E-01	1.0810E-01	1.2467E-02	0.0000E+00

$$\underline{u}^T = [\delta b\ \delta r\ \delta s_1\ \delta_2]$$

B MATRIX

-1.6315E-03	-5.8396E-02	2.8022E-03	2.8022E-03
0.0000E+00	2.3119E+00	-1.6950E-01	1.6950E-01
-1.4442E+00	-1.4815E-06	-9.8476E-01	-9.8476E-01
0.0000E+00	4.2586E-02	2.0848E-01	-2.0848E-01
1.3872E-02	4.8862E-07	-2.3825E-02	-2.3825E-02
0.0000E+00	-5.8593E-02	-3.3676E-04	3.3676E-04
0.0000E+00	0.0000E+00	0.0000E+00	0.0000E+00
0.0000E+00	0.0000E+00	0.0000E+00	0.0000E+00